frontiers | Frontiers in Materials

ORIGINAL RESEARCH
published: 08 April 2022
doi: 10.3389/fmats.2022.855950

Band-Gap and Dimensional Engineering in Lead-Free Inorganic Halide Double Perovskite $Cs_4Cu_{1-x}Ag_{2x}Sb_2Cl_{12}$ Single Crystals and Nanocrystals

Wei Zhou[1†], *Peigeng Han*[2*†], *Cheng Luo*[3,4], *Cheng Li*[1], *Jie Hou*[3,4], *Yang Yu*[1*] and *Ruifeng Lu*[1*]

[1]Department of Applied Physics & MIIT Key Laboratory of Semiconductor Microstructure and Quantum Sensing, Institute of Ultrafast Optical Physics, Nanjing University of Science and Technology, Nanjing, China, [2]Institute of Molecular Sciences and Engineering, Institute of Frontier and Interdisciplinary Science, Shandong University, Qingdao, China, [3]State Key Laboratory of Molecular Reaction Dynamics, Dalian Institute of Chemical Physics, Chinese Academy of Science, Dalian, China, [4]University of the Chinese Academy of Sciences, Beijing, China

Lead free double perovskites (DPs) are promising materials due to their non-toxic and tunable optical properties. In this work, a series of lead-free halide DP single crystals (SCs) and nanocrystals (NCs) ($Cs_4Cu_{1-x}Ag_{2x}Sb_2Cl_{12}$) were reported. With alloying strategy, the optical band-gap engineering was realized and the dimension can be controlled between 2D and 3D. The Cu-alloyed SCs exhibit strong absorption from the UV-visible region to the near-infrared range (can even completely cover the bands of NIR-I and NIR-II). In addition, ($Cs_4Cu_{1-x}Ag_{2x}Sb_2Cl_{12}$) NCs were synthesized via a top-down approach, which maintains similar optical properties and the dimensional transformation phenomenon to SCs. These results suggest the great potential of $Cs_4Cu_{1-x}Ag_{2x}Sb_2Cl_{12}$ SCs and NCs for photovoltaic and optoelectronic applications.

Keywords: lead-free double perovskite, alloying strategy, band-gap engineering, dimensional engineering, light absorbing material

OPEN ACCESS

Edited by:
Zao Yi,
Southwest University of Science and Technology, China

Reviewed by:
Yougen Yi,
Central South University, China
Hua Yang,
Lanzhou University of Technology, China
Xianpei Ren,
Sichuan University of Science and Engineering, China

***Correspondence:**
Peigeng Han
hanpeigeng@sdu.edu.cn
Yang Yu
yuyang2019@njust.edu.cn
Ruifeng Lu
rflu@njust.edu.cn

†*These authors have contributed equally to this work*

Specialty section:
This article was submitted to Semiconducting Materials and Devices, a section of the journal Frontiers in Materials

Received: *16 January 2022*
Accepted: *09 February 2022*
Published: *08 April 2022*

Citation:
Zhou W, Han P, Luo C, Li C, Hou J, Yu Y and Lu R (2022) Band-Gap and Dimensional Engineering in Lead-Free Inorganic Halide Double Perovskite $Cs_4Cu_{1-x}Ag_{2x}Sb_2Cl_{12}$ Single Crystals and Nanocrystals. Front. Mater. 9:855950. doi: 10.3389/fmats.2022.855950

INTRODUCTION

Lead perovskites have attracted widespread attention for their high charge carrier mobility, adjustable photoluminescence peak, and appropriate band gap. However, the toxicity of lead is a threat to the biosphere and the poor stability hinders its large-scale commercial application (Nedelcu et al., 2015; Park et al., 2015; Protesescu et al., 2015; Song et al., 2015; Yakunin et al., 2015). Due to their environment friendly properties and good photoelectric performance, lead free perovskite has been frequently reported in recent years. Isovalent Sn^{2+} is used to replace Pb^{2+}, the $CsSnX_3$ (X = Cl, Br, I) perovskites retain excellent optical properties and 3D crystal structure (Jellicoe et al., 2016). However, due to the easy oxidation of Sn^{2+} to Sn^{4+}, these perovskites suffer from poor stability (Wang et al., 2016). There are also reports of lead-free DPs $Cs_2B'BCl_6$ (B′=Ag, Na; B=In, Sc, Bi, Er), which have high stability, 3D crystal structure, and efficient photoluminescence (PL). Their PL quantum yields (PLQYs) scan be further enhanced by doping or alloying strategy (Luo et al., 2018; Han et al., 2019a; Han et al., 2019b; Liu et al., 2021; Wu R et al., 2021; Zhang et al., 2021).

Although the development of the lead-free double perovskites (DPs) has made phased progress, to date, there are still many shortcomings that need to be remedied: 1) For lead-free DPs, present research

mainly focuses on 3D structure SCs and NCs, but there are few studies on 2D perovskites and the regulation of their dimensions (Luo et al., 2018; Han et al., 2019b). 2) In addition to PL properties, lead-free perovskites can also be used as light-absorbing materials. At present, most of the reported lead-free DPs have a large band gap and their absorption spectra is mostly in the ultraviolet region, which cannot make full use of the photons in the visible and near-infrared regions (Han et al., 2019a; Manna and Xia, 2021). The narrow absorption spectra region hinders their further application in the field of photovoltaic (Wu X et al., 2021; Zheng et al., 2022). Recently, $Cs_2AgBiBr_6$ SC was reported and used in fields of photovoltage and photoelectric devices (Slavney et al., 2016; Greul et al., 2017; Pan et al., 2017). Our group reported a series of lead-free iron-based halide DP $Cs_2Ag_xNa_{1-x}FeCl_6$ with a small tunable band-gap from 1.78 to 2.33 eV and $Cs_2CuSbCl_6$ NCs with a small band gap of 1.66 eV (Zhou et al., 2020; Han et al., 2021). However, there are few reports about lead-free perovskites that extend the absorption from the UV-visible region to the NIR range to make full utilization of the sun's light. The design and synthesis of lead-free perovskite that can broaden the absorption spectra to the NIR region with adjustable optical band gap and high stability are of great benefit to photovoltaic and optoelectronic applications. Vargas et al. have synthesized a layered Cu(II)-Sb-based DP SC with a small band gap (Vargas, Ramos et al., 2017). Furthermore, the layered Cu(II)-Sb-based DP NCs have exhibited excellent optoelectronic response performance (Wang et al., 2019; Cai et al., 2020). Inspired by these works, we have tried to develop a series of lead-free inorganic DP SCs and NCs with adjustable band gap and controllable structure dimension through alloying strategy.

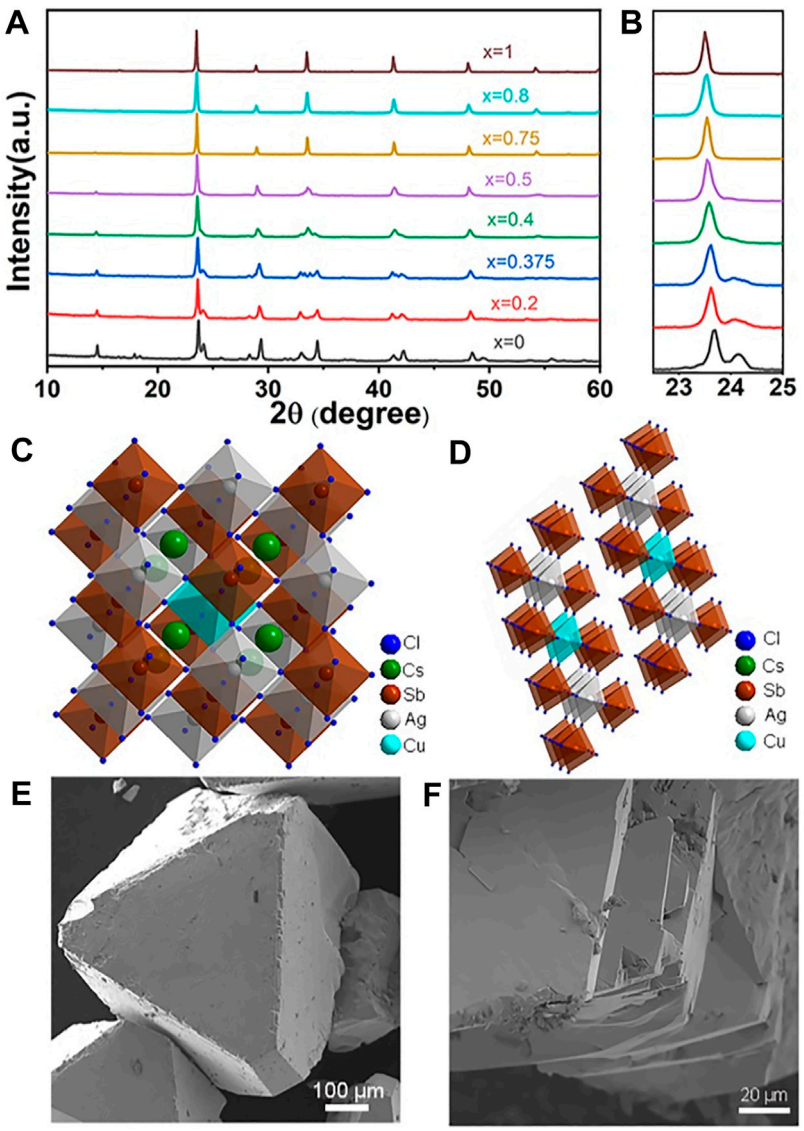

FIGURE 1 | (A) XRD patterns of $Cs_4Cu_{1-x}Ag_{2x}Sb_2Cl_{12}$ (x = 0, 0.2, 0.25, 0.4, 0.5, 0.75, 0.8, 1). **(B)** Magnified images of (022) diffraction peaks. **(C,D)** Crystal structures of $Cs_4Cu_{1-x}Ag_xSb_2Cl_{12}$ (x > 0.5 **(C)**, x < 0.4 **(D)**). **(E,F)** SEM images of $Cs_4Cu_{1-x}Ag_xSb_2Cl_{12}$ SCs (x = 0.75 **(E)**, x = 0.2 **(F)**).

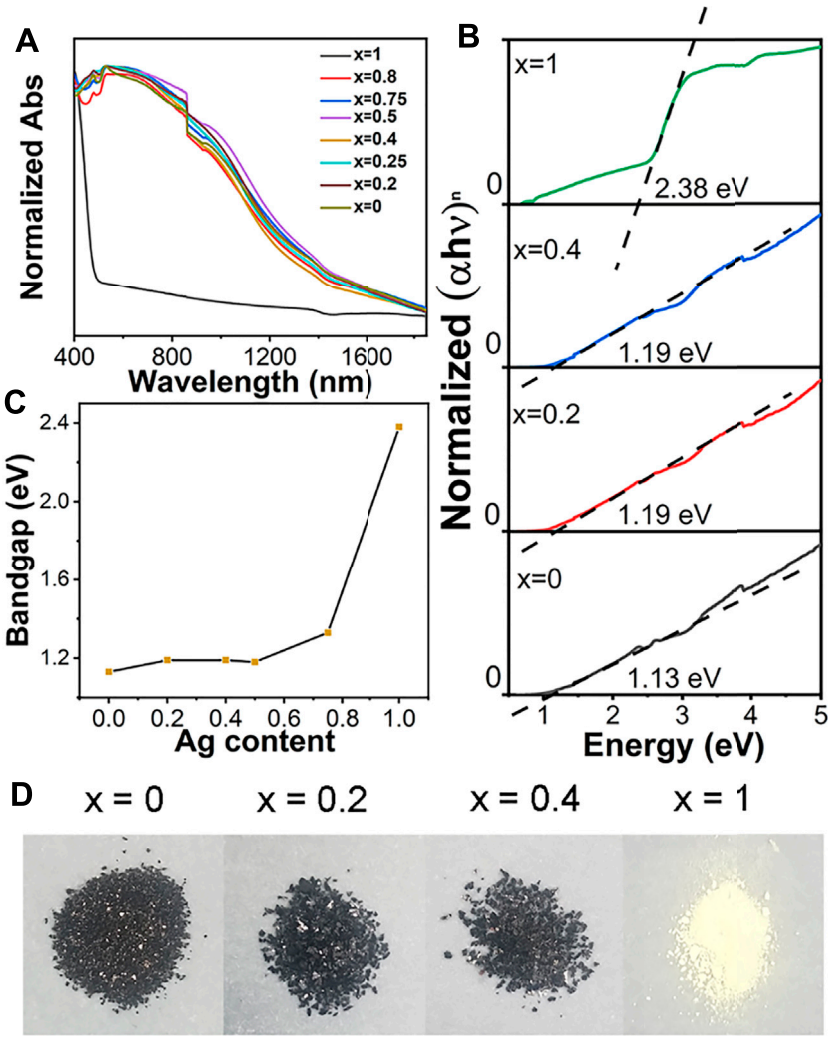

FIGURE 2 | (A) Steady-state absorption spectra of $Cs_4Cu_{1-x}Ag_{2x}Sb_2Cl_{12}$ (x = 0, 0.2, 0.25, 0.4, 0.5, 0.75, 0.8, 1) SCs. **(B)** Tauc plots of $Cs_4Cu_{1-x}Ag_{2x}Sb_2Cl_{12}$ SCs. (x = 1: $n = \frac{1}{2}$; x = 0, 0.2, 0.4: $n = 2$) **(C)** Correlation between Ag content and band gap value of $Cs_4Cu_{1-x}Ag_{2x}Sb_2Cl_{12}$ SCs. **(D)** Photographs of $Cs_4Cu_{1-x}Ag_{2x}Sb_2Cl_{12}$ (x = 0, 0.2, 0.4, 1) SCs.

Herein, $Cs_4Cu_{1-x}Ag_{2x}Sb_2Cl_{12}$ SCs and NCs were synthesized. All the Cu alloyed samples showed strong absorption in the visible region and near infrared (NIR) region (including NIR I and NIR II). The alloying strategy can tune the optical band gap, and effectively control the structure dimension of this system. With the increase of Ag content, a shift of the structure from 2D to 3D can be realized. A blue shift of the absorption edge of the NCs was shown compared to the corresponding SCs. In addition, the stability of these SCs was also studied.

EXPERIMENTAL METHODS

Materials

Cesium chloride (CsCl, 99%, Aladdin), copper chloride ($CuCl_2$, 99.99%, Alfa Aesar), silver chloride (AgCl, 99.9%, Alfa Aesar), antimonous chloride ($SbCl_3$, 99.9%, Alfa Aesar), hydrochloric acid (analytical pure, Sinopharm Chemical Reagent Co., Ltd., China), n-hexane (97%, Aladdin), toluene (99.5%, Sinopharm Chemical Reagent Co., Ltd., China). All chemicals are used as received without further purification.

Synthesis of $Cs_4Cu_{1-x}Ag_{2x}Sb_2Cl_{12}$ ($0 \leq x \leq 1$) Single Crystals by Hydrothermal Method

For the $Cs_4Cu_{1-x}Ag_{2x}Sb_2Cl_{12}$ (x = 0, 0.2, 0.25, 0.4, 0.5, 0.75,0.8 and 1) SCs, 4 mmol CsCl, 2 mmol $SbCl_3$, 2x mmol AgCl and 1-x mmol $CuCl_2$ were dissolved in 10 ml hydrobromic acid in a 20 ml Teflon liner. Then, it was heated at 180°C for 16 h in a stainless steel Parr autoclave and was slowly cooled to room temperature (RT) at a speed of 5–8°C/h. Finally, the SCs were filtered and dried in vacuum at 70°C for 10 h.

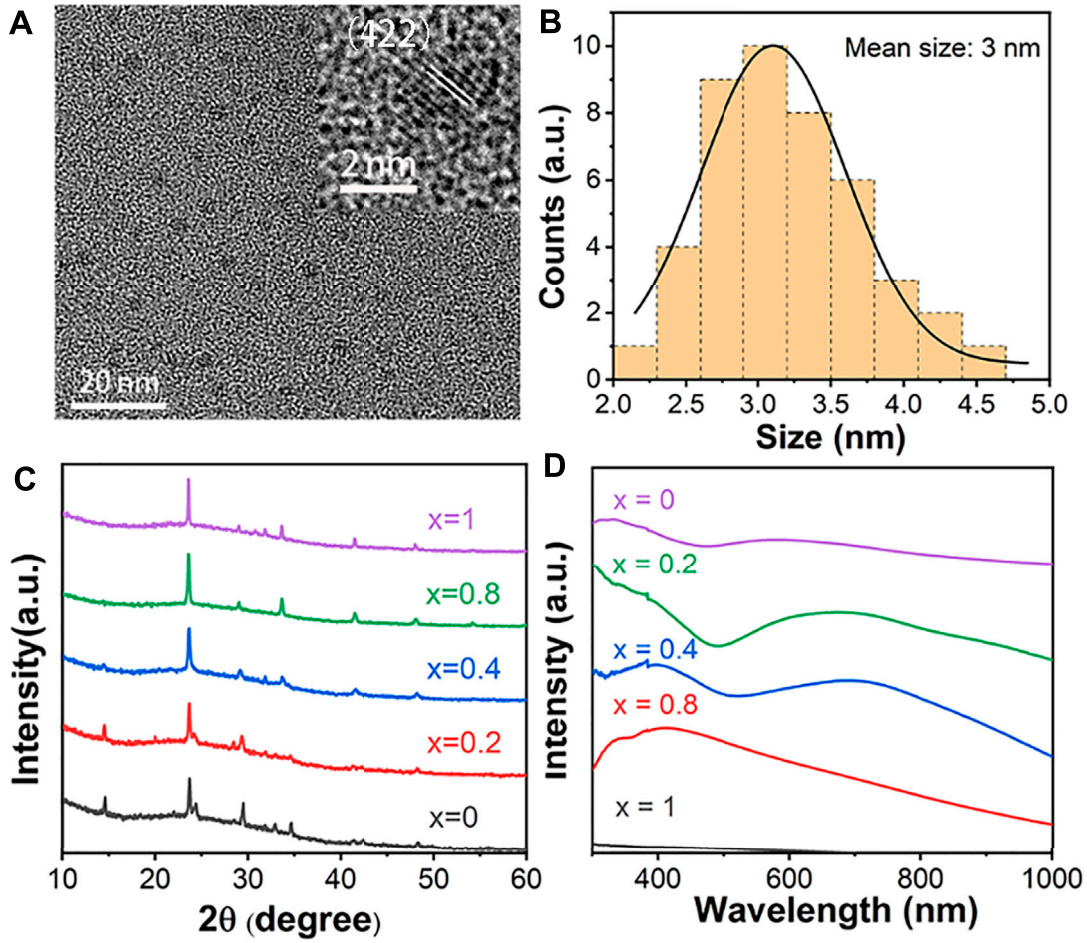

FIGURE 3 | (A) TEM and HRTEM (insert) images of $Cs_4Cu_{0.2}Ag_{1.6}Sb_2Cl_{12}$ NCs. **(B)** The size distribution histogram of $Cs_4Cu_{0.2}Ag_{1.6}Sb_2Cl_{12}$ NCs. **(C)** XRD patterns of $Cs_4Cu_{1-x}Ag_{2x}Sb_2Cl_{12}$ (x = 0, 0.2, 0.4, 0.8, 1) NCs. **(D)** Absorption spectra of $Cs_4Cu_{1-x}Ag_{2x}Sb_2Cl_{12}$ (x = 0, 0.2, 0.4, 0.8, 1) NCs.

Synthesis of $Cs_4Cu_{1-x}Ag_{2x}Sb_2Cl_{12}$ (x = 0, 0.2, 0.4, 0.8, and 1) Nanocrystals by Ultrasonic Crushing Method

The SCs were ground into a micron-sized powder. The powder (0.04 g) was added to 10 ml hexane, which was ultrasonicated by an ultrasonic probe (Scientz-IID, 300 W, ultrasonic homogenizer, Ningbo, China) for 20 min at 60°C. Then, the solution was centrifuged for 5 min at 1,000 rpm/min to discard the large crystals and the supernatant solution containing the NCs was obtained. After this, the colloidal NCs solution was further centrifuged for 5 min at 5,000 rpm/min to obtain the NCs precipitate for further characterization.

Structural Characterizations

Powder X-ray diffraction (PXRD) was performed on a PANalytical Empyrean diffractometer equipped with Cu Kα X-ray (λ = 1.54056 Å) tubes, and the acquisition was done for every 0.04° increment. A field emission scanning electron microscope (FESEM, JEOL, JSM-7800F, 3kV) equipped with an Oxford X-Max silicon drift detector was used to record the surface morphology and perform chemical analysis. The transmission electron microscopy (TEM) measurements were performed by using the JEM-2100. Thermogravimetric analysis (TGA) thermogram was operated under a nitrogen atmosphere with a Netzsch STA 449 F3Jupiter thermo-microbalance at a heating rate of 10°C/min.

Optical Absorption Spectroscopy

For colloidal NCs, steady-state optical absorption measurement was performed by using the PerkinElmer Lambda 35 double-beam spectrometer equipped with integrating sphere to exclude signal due to light scattering. For single crystal powder, steady-state absorption spectra were recorded using a UV–vis (SHIMADZU UV2600) spectrometer. Optical diffuse reflectance measurements were performed by equipping it with an integrating sphere at room temperature and $BaSO_4$ as the 100% reflectance reference. The reflectance data are converted to absorption according to the Kubelka–Munk equation, $F(R) = (1-R)^2(2R)^{-1} = \alpha/S$, where R is the reflectance, α and S are the absorption and scattering coefficients, respectively.

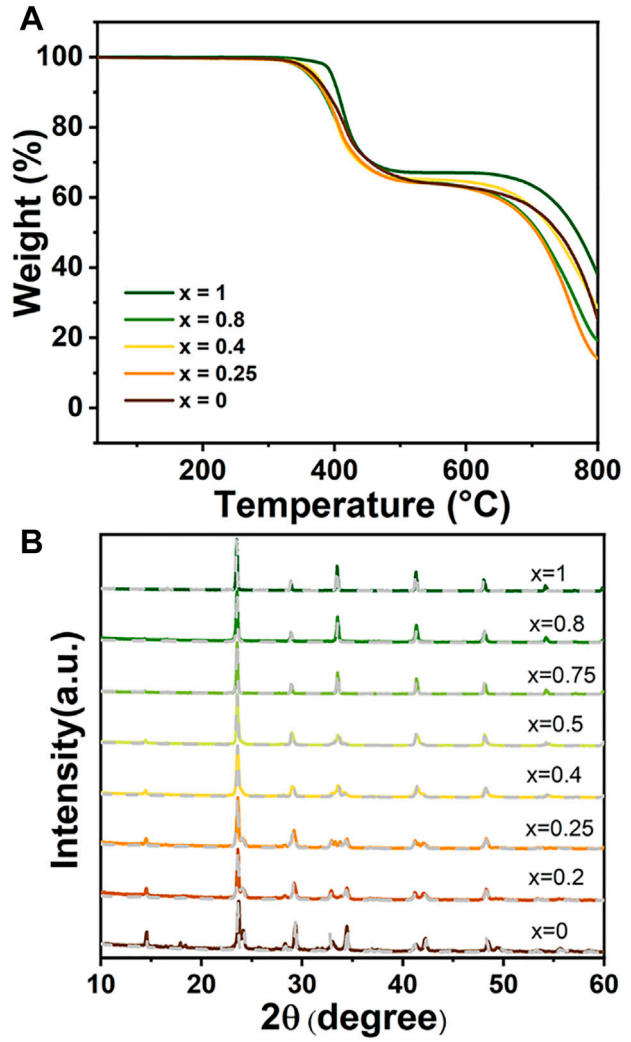

FIGURE 4 | (A) TGA of $Cs_4Cu_{1-x}Ag_{2x}Sb_2Cl_{12}$ (x = 0, 0.2, 0.4, 0.8, 1) SCs. **(B)** XRD patterns of as-synthesized $Cs_4Cu_{1-x}Ag_{2x}Sb_2Cl_{12}$ (x = 0, 0.2, 0.4, 0.8, 1) SCs (gray dashed line) compared to corresponding samples after exposure to ambient air for 3 months.

RESULTS AND DISCUSSION

As shown in the PXRD pattern (**Figure 1A**, **B**), the $Cs_2AgSbCl_6$ (x=1) adopts a highly symmetric cubic DP structure with Fm-3m space symmetry. The cubic DP structure is maintained from x =1 to x = 0.75 (**Figure 1C**). For the Ag-Cu alloyed samples, two Ag atoms were replaced by one Cu atom and one vacancy. With the increase of Cu amount, due to the lattice contraction caused by smaller Cu^{2+} ionic radius than Ag^+, the diffraction peak slightly shifted to higher 2θ values from x = 1 to 0. The expansion and splitting of the diffraction peak around 23.7° also appeared with the decreasing of x, corresponding to the structure change. The $Cs_4CuSb_2Cl_{12}$ shows a vacancy ordered layered DP crystal structure and this structure was maintained from x = 0 to x = 0.4 (**Figure 1D**) (Vargas et al., 2017). The changes of crystal structure with different ratios of Ag/Cu can also be shown by the scanning electron microscopy (SEM) results. The $Cs_4Cu_{1-x}Ag_{2x}Sb_2Cl_{12}$ (x = 0.75, 0.8) SCs possessed significant three-dimensional octahedral structure with grain sizes around 0.7 mm (**Figure 1E**; **Supplementary Figure S1A**). When Cu reached a higher content (x < 0.4), the SEM images showed a layered 2D morphology (**Figure 1F**; **Supplementary Figure S1B**). Energy-dispersive X-ray spectroscopy (EDS) analysis was performed to obtain the actual alloying amounts (**Supplementary Table S1**). The results showed that the actual Cu and Ag contents were generally consistent with the feeding ratios. The EDS elemental mappings of $Cs_4Cu_{0.8}Ag_{0.4}Sb_2Cl_{12}$ SCs visually reveal the homogeneous distribution of Cs, Ag, Cu, Sb, Cl (**Supplementary Figure S2**).

To characterize the optical properties of $Cs_4Cu_{1-x}Ag_{2x}Sb_2Cl_{12}$ (x = 0, 0.2, 0.25, 0.4, 0.5, 0.75, 0.8, 1) SCs, we measured steady-state absorption spectra, as shown in **Figure 2A**. The unalloyed $Cs_2AgSbCl_6$ SCs have narrow absorption in the ultraviolet region. All the Cu alloyed samples and pure $Cs_4CuSb_2Cl_{12}$ SCs exhibit strong absorption from the UV-visible region to the near-infrared range (can even completely cover the bands of NIR-I and NIR-II), which shows great potential as light absorption materials. The Tauc plot of $Cs_2AgSbCl_6$ SCs shows a wide band gap of 2.38 eV (by assuming an indirect band gap) and the band gap of $Cs_4Cu_{1-x}Ag_xSb_2Cl_{12}$ (x = 0, 0.2, 0.4) SCs are 1.13, 1.19, and 1.19 eV (by assuming a direct band gap). The transition from a wide indirect band gap to a narrow direct band gap is successfully realized through the alloying strategy. The correlation between Ag content and band gap value of $Cs_4Cu_{1-x}Ag_{2x}Sb_2Cl_{12}$ SCs is shown in **Figure 2C**. The band gap decreases with the decline in x. In the range of $0.5 < x \leq 1$, the variation of band gap is very sensitive to the change of x. But when $x \leq 0.5$, the band gap hardly changes with the decrease of x (the slope is gentle). The color of $Cs_2AgSbCl_6$ SCs are cream-yellow while all the Cu alloyed SCs are black, which correspond to the absorption spectra (**Figure 2D**).

Due to the quantum confinement effect, it is expected that $Cs_4Cu_{1-x}Ag_{2x}Sb_2Cl_{12}$ (x = 0, 0.2, 0.25, 0.4, 0.5, 0.75, 0.8, 1) halide DP with nanoscale size will have special optical properties and show great potential in optoelectronic devices (Cheng et al., 2022). In addition, NCs have greater advantages than SCs in many fields, such as thin film preparation and flexible device fabrication (Shamsi et al., 2019; Zhang et al., 2020; Song et al., 2021). In this paper, top-down ultrasonic crushing method was adopted to synthesize the $Cs_4Cu_{1-x}Ag_{2x}Sb_2Cl_{12}$ (x = 0, 0.2, 0.4, 0.8, 1) NCs. The photograph of $Cs_4Cu_{1-x}Ag_{2x}Sb_2Cl_{12}$ (x = 1, 0.2, 0.4, 0.8, and 0) colloidal NCs are presented in **Supplementary Figure S3**. **Figure 3A** shows the TEM image of $Cs_4Cu_{0.2}Ag_{1.6}Sb_2Cl_{12}$ NCs, which have a relatively even distribution with an average diameter of 3 nm (**Figure 3B**). These NCs obtained by ultrasonic crushing method mostly exhibit a near-spherical shape. From a high-resolution TEM (HRTEM) image of the $Cs_4Cu_{0.2}Ag_{1.6}Sb_2Cl_{12}$ NCs (insert of **Figure 3A**), the lattice fringes can be clearly observed. PXRD measurements were also performed (**Figure 3C**). With the increasing of Cu content, the diffraction peak shifted slightly to the right, which is caused by the decreasing lattice parameters caused by smaller Cu^{2+} ionic radius than Ag^+. The diffraction

peak around 23.7° shows expansion and splitting in the XRD patterns of $Cs_4Cu_{1-x}Ag_{2x}Sb_2Cl_{12}$ (x = 0, 0.2) NCs. The expansion and splitting of the diffraction peak correspond with the change of structure and is consistent with the result of SCs. Combining the results of both PXRD and TEM, it can be proved that all the $Cs_4Cu_{1-x}Ag_{2x}Sb_2Cl_{12}$ (x = 0, 0.2, 0.4, 0.8, 1) NCs possess high crystallinity, single pure phase, and uniform nanoparticle size. Steady-state absorption spectra were also measured to characterize the optical properties (**Figure 3D**). $Cs_2AgSbCl_6$ NCs have very weak absorption in the visible wavelength range. With the introduction of Cu, all the Cu-alloyed $Cs_4Cu_{1-x}Ag_xSb_2Cl_{12}$ (x = 0, 0.2, 0.4, 0.8) NCs have an intense and wide absorption containing the entire visible and the partial NIR regions. The $Cs_4CuSb_2Cl_{12}$ NCs exhibit a broad absorption peak centered at 580 nm, which is slightly blue-shifted compared to the corresponding SCs.

Stability is also one of the important criteria to evaluate the quality of light-absorbing materials (Niu et al., 2015; Stranks and Snaith, 2015). The thermal stability and air stability of these SCs and NCs were further measured. The TGA result of SCs is presented in **Figure 4A**. The $Cs_4Cu_{1-x}Ag_xSb_2Cl_{12}$ (x = 0, 0.2, 0.4, 0.8, and 1) SCs exhibit an excellent thermal stability at high temperature and no weight loss until 330°C. The PXRD patterns of $Cs_4Cu_{1-x}Ag_{2x}Sb_2Cl_{12}$ (x = 0, 0.2, 0.4, 0.8, 1) SCs stored in air for 3 months was also measured to study the air stability (**Figure 4B**). Compared to synthesized SCs (gray dashed line), no obvious diffraction peaks of impurity were observed, which confirms that the $Cs_4Cu_{1-x}Ag_{2x}Sb_2Cl_{12}$ (x = 0, 0.2, 0.4, 0.8, 1) SCs have excellent air stability. The TGA result of NCs show excellent thermal stability at high temperature (**Supplementary Figure S4A**). The colloidal NCs solutions are stored in ambient air for 1 month and also show good air stability (**Supplementary Figure S4B**).

CONCLUSION

In conclusion, a series of inorganic Cu-Ag alloyed DP SCs were designed and successfully synthesized. The absorption spectra of the alloyed SCs include the whole visible to partial NIR (NIR-I and NIR-II) region. The changing the ratios of Ag/Cu can achieve the transition of band structure from indirect to direct, the adjustment of band gap value, and the transformation of crystal dimension from 3D to 2D. Then, we extend the synthesis to the nanoscale through the ultrasonic crushing method and further study the optical properties of colloidal NCs. These NCs maintain similar light absorption properties to the SCs. Our work highlights that these lead-free halide DP SCs display not only excellent photoelectronic properties but also high stability, which provides an ideal choice for light absorption materials. This alloying strategy will greatly push the development of lead-free metal halide DPs and widen its applications in photovoltaic and optoelectronic devices.

DATA AVAILABILITY STATEMENT

The original contributions presented in the study are included in the article/**Supplementary Material**, further inquiries can be directed to the corresponding authors.

AUTHOR CONTRIBUTIONS

PH grew the perovskite SCs. WZ synthesized the perovskite NCs. CLu, CLi and JH did the measurements. WZ, PH and YY analyzed the results. WZ wrote the manuscript. RL designed the experiment and revised the manuscript. All authors made comments on this manuscript.

FUNDING

This work was supported by the National Key Research and Development Program of China (grant 2017YFA0204800), the National Natural Science Foundation of China (grant Nos. 21833009 and 52002182), the Natural Science Foundation of Jiangsu Province (grant No. BK20170032), the Scientific Instrument Developing Project of the Chinese Academy of Sciences (grant No. YJKYYQ20190003).

SUPPLEMENTARY MATERIAL

The Supplementary Material for this article can be found online at: https://www.frontiersin.org/articles/10.3389/fmats.2022.855950/full#supplementary-material

REFERENCES

Cai, T., Shi, W., Hwang, S., Kobbekaduwa, K., Nagaoka, Y., Yang, H., et al. (2020). Lead-free Cs4CuSb2Cl12 Layered Double Perovskite Nanocrystals. *J. Am. Chem. Soc.* 142 (27), 11927–11936. doi:10.1021/jacs.0c04919

Cheng, T., Gao, H., Liu, G., Pu, Z., Wang, S., Yi, Z., et al. (2022). Preparation of Core-Shell Heterojunction Photocatalysts by Coating CdS Nanoparticles onto $Bi_4Ti_3O_{12}$ Hierarchical Microspheres and Their Photocatalytic Removal of Organic Pollutants and Cr(VI) Ions. *Colloids Surf. A: Physicochemical Eng. Aspects* 633, 127918. doi:10.1016/j.colsurfa.2021.127918

Greul, E., Petrus, M. L., Binek, A., Docampo, P., and Bein, T. (2017). Highly Stable, Phase Pure Cs2AgBiBr6 Double Perovskite Thin Films for Optoelectronic Applications. *J. Mater. Chem. A.* 5 (37), 19972–19981. doi:10.1039/c7ta06816f

Han, P., Luo, C., Zhou, W., Hou, J., Li, C., Zheng, D., et al. (2021). Band-gap Engineering of lead-free Iron-Based Halide Double-Perovskite Single Crystals and Nanocrystals by an Alloying or Doping Strategy. *J. Phys. Chem. C* 125 (21), 11743–11749. doi:10.1021/acs.jpcc.1c02636

Han, P., Mao, X., Yang, S., Zhang, F., Yang, B., Wei, D., et al. (2019a). Lead-Free Sodium-Indium Double Perovskite Nanocrystals through Doping Silver Cations for Bright Yellow Emission. *Angew. Chem. Int. Ed.* 58 (48), 17231–17235. doi:10.1002/anie.201909525

Han, P., Zhang, X., Mao, X., Yang, B., Yang, S., Feng, Z., et al. (2019b). Size Effect of lead-free Halide Double Perovskite on Luminescence Property. *Sci. China Chem.* 62 (10), 1405–1413. doi:10.1007/s11426-019-9520-1

Jellicoe, T. C., Richter, J. M., Glass, H. F. J., Tabachnyk, M., Brady, R., Dutton, S. E., et al. (2016). Synthesis and Optical Properties of lead-free Cesium Tin Halide Perovskite Nanocrystals. *J. Am. Chem. Soc.* 138 (9), 2941–2944. doi:10.1021/jacs.5b13470

Liu, Y., Nag, A., Manna, L., and Xia, Z. (2021). Lead-Free Double Perovskite Cs 2 AgInCl 6. *Angew. Chem. Int. Ed.* 60 (21), 11592–11603. doi:10.1002/anie.202011833

Luo, J., Wang, X., Li, S., Liu, J., Guo, Y., Niu, G., et al. (2018). Efficient and Stable Emission of Warm-white Light from lead-free Halide Double Perovskites. *Nature* 563 (7732), 541–545. doi:10.1038/s41586-018-0691-0

Nedelcu, G., Protesescu, L., Yakunin, S., Bodnarchuk, M. I., Grotevent, M. J., and Kovalenko, M. V. (2015). Fast Anion-Exchange in Highly Luminescent Nanocrystals of Cesium Lead Halide Perovskites ($CsPbX_3$, X = Cl, Br, I). *Nano Lett.* 15 (8), 5635–5640. doi:10.1021/acs.nanolett.5b02404

Niu, G., Guo, X., and Wang, L. (2015). Review of Recent Progress in Chemical Stability of Perovskite Solar Cells. *J. Mater. Chem. A.* 3 (17), 8970–8980. doi:10.1039/C4TA04994B

Pan, W., Wu, H., Luo, J., Deng, Z., Ge, C., Chen, C., et al. (2017). Cs2AgBiBr6 Single-crystal X-ray Detectors with a Low Detection Limit. *Nat. Photon* 11 (11), 726–732. doi:10.1038/s41566-017-0012-4

Park, Y.-S., Guo, S., Makarov, N. S., and Klimov, V. I. (2015). Room Temperature Single-Photon Emission from Individual Perovskite Quantum Dots. *ACS Nano* 9 (10), 10386–10393. doi:10.1021/acsnano.5b04584

Protesescu, L., Yakunin, S., Bodnarchuk, M. I., Krieg, F., Caputo, R., HendonKovalenko, C. H., et al. (2015). Nanocrystals of Cesium Lead Halide Perovskites ($CsPbX_3$, X = Cl, Br, and I): Novel Optoelectronic Materials Showing Bright Emission with Wide Color Gamut. *Nano Lett.* 15 (6), 3692–3696. doi:10.1021/nl5048779

Shamsi, J., Urban, A. S., Imran, M., De Trizio, L., and Manna, L. (2019). Metal Halide Perovskite Nanocrystals: Synthesis, post-synthesis Modifications, and Their Optical Properties. *Chem. Rev.* 119 (5), 3296–3348. doi:10.1021/acs.chemrev.8b00644

Slavney, A. H., Hu, T., Lindenberg, A. M., and Karunadasa, H. I. (2016). A Bismuth-Halide Double Perovskite with Long Carrier Recombination Lifetime for Photovoltaic Applications. *J. Am. Chem. Soc.* 138 (7), 2138–2141. doi:10.1021/jacs.5b13294

Song, J.-K., Kim, M. S., Yoo, S., Koo, J. H., and Kim, D.-H. (2021). Materials and Devices for Flexible and Stretchable Photodetectors and Light-Emitting Diodes. *Nano Res.* 14 (9), 2919–2937. doi:10.1007/s12274-021-3447-3

Song, J., Li, J., Li, X., Xu, L., Dong, Y., and Zeng, H. (2015). Quantum Dot Light-Emitting Diodes Based on Inorganic Perovskite Cesium Lead Halides ($CsPbX_3$). *Adv. Mater.* 27 (44), 7162–7167. doi:10.1002/adma.201502567

Stranks, S. D., and Snaith, H. J. (2015). Metal-halide Perovskites for Photovoltaic and Light-Emitting Devices. *Nat. Nanotech* 10 (5), 391–402. doi:10.1038/nnano.2015.90

Vargas, B., Ramos, E., Pérez-Gutiérrez, E., Alonso, J. C., and Solis-Ibarra, D. (2017). A Direct Bandgap Copper-Antimony Halide Perovskite. *J. Am. Chem. Soc.* 139 (27), 9116–9119. doi:10.1021/jacs.7b04119

Wang, A., Yan, X., Zhang, M., Sun, S., Yang, M., Shen, W., et al. (2016). Controlled Synthesis of Lead-Free and Stable Perovskite Derivative Cs2SnI6 Nanocrystals via a Facile Hot-Injection Process. *Chem. Mater.* 28 (22), 8132–8140. doi:10.1021/acs.chemmater.6b01329

Wang, X.-D., Miao, N.-H., Liao, J.-F., Li, W.-Q., Xie, Y., Chen, J., et al. (2019). The Top-Down Synthesis of Single-Layered Cs4CuSb2Cl12 Halide Perovskite Nanocrystals for Photoelectrochemical Application. *Nanoscale* 11 (12), 5180–5187. doi:10.1039/C9NR00375D

Wu, R., Han, P., Zheng, D., Zhang, J., Yang, S., Zhao, Y., et al. (2021). All-Inorganic Rare-Earth-Based Double Perovskite Nanocrystals with Near-Infrared Emission. *Laser Photon. Rev.* 15 (11), 2100218. doi:10.1002/lpor.202100218

Wu, X., Zheng, Y., Luo, Y., Zhang, J., Yi, Z., Wu, X., et al. (2021). A Four-Band and Polarization-independent BDS-Based Tunable Absorber with High Refractive index Sensitivity. *Phys. Chem. Chem. Phys.* 23 (47), 26864–26873. doi:10.1039/D1CP04568G

Yakunin, S., Protesescu, L., Krieg, F., Bodnarchuk, M. I., Nedelcu, G., Humer, M., et al. (2015). Low-threshold Amplified Spontaneous Emission and Lasing from Colloidal Nanocrystals of Caesium lead Halide Perovskites. *Nat. Commun.* 6 (1), 8056. doi:10.1038/ncomms9056

Zhang, J., Zhang, W., Cheng, H.-M., and Silva, S. R. P. (2020). Critical Review of Recent Progress of Flexible Perovskite Solar Cells. *Mater. Today* 39, 66–88. doi:10.1016/j.mattod.2020.05.002

Zhang, R., Wang, Z., Xu, X., Mao, X., Xiong, J., Yang, Y., et al. (2021). All-Inorganic Rare-Earth Halide Double Perovskite Single Crystals with Highly Efficient Photoluminescence. *Adv. Opt. Mater.* 9 (19), 2100689. doi:10.1002/adom.202100689

Zheng, Z., Zheng, Y., Luo, Y., Yi, Z., Zhang, J., Liu, Z., et al. (2022). A Switchable Terahertz Device Combining Ultra-wideband Absorption and Ultra-wideband Complete Reflection. *Phys. Chem. Chem. Phys.* 24 (4), 2527–2533. doi:10.1039/D1CP04974G

Zhou, W., Han, P., Zhang, X., Zheng, D., Yang, S., Yang, Y., et al. (2020). Lead-free Small-Bandgap $Cs_2CuSbCl_6$ Double Perovskite Nanocrystals. *J. Phys. Chem. Lett.* 11 (15), 6463–6467. doi:10.1021/acs.jpclett.0c01968

Conflict of Interest: The authors declare that the research was conducted in the absence of any commercial or financial relationships that could be construed as a potential conflict of interest.

Publisher's Note: All claims expressed in this article are solely those of the authors and do not necessarily represent those of their affiliated organizations or those of the publisher, the editors and the reviewers. Any product that may be evaluated in this article, or claim that may be made by its manufacturer, is not guaranteed or endorsed by the publisher.